Soft Matter

Nonequilibrium interactions between multi-scale colloids regulate the suspension microstructure and rheology

Journal:	*Soft Matter*
Manuscript ID	SM-ART-07-2023-000947.R1
Article Type:	Paper
Date Submitted by the Author:	28-Sep-2023
Complete List of Authors:	Xu, Yaxin; University of California Santa Barbara, Chemical Engineering Takatori, Sho; University of California Santa Barbara, Department of Chemical Engineering

Soft Matter

ARTICLE TYPE

Cite this: DOI: 00.0000/xxxxxxxxxx

Nonequilibrium interactions between multi-scale colloids regulate the suspension microstructure and rheology

Yaxin Xu[a] and Sho C. Takatori[a‡]

Received Date
Accepted Date

DOI: 00.0000/xxxxxxxxxx

Understanding nonequilibrium interactions of multi-component colloidal suspensions is critical for many dynamical settings such as self assembly and material processing. A key question is how the nonequilibrium distributions of individual components influence the effective interparticle interactions and flow behavior. In this work, we develop a first-principle framework to study a bidisperse suspension of colloids and depletants using a Smoluchowski equation and corroborated by Brownian Dynamics (BD) simulations. Using nonlinear microrheology as a case study, we demonstrate that effective depletion interactions between driven colloids are sensitive to particle timescales out of equilibrium and cannot be predicted by equilibrium-based pair potentials like Asakura-Oosawa. Furthermore, we show that the interplay between Brownian relaxation timescales of different species plays a critical role in governing the viscosity of multi-component suspensions. Our model highlights the limitations of using equilibrium pair potentials to approximate interparticle interactions in nonequilibrium processes such as hydrodynamic flows and presents a useful framework for studying the transport of driven, interacting suspensions.

1 Introduction

When a colloidal suspension is driven out of equilibrium by body forces or hydrodynamic flows, interactions between the individual particles can couple with convective forces to induce microstructural reorganizations and relaxations across large time and length scales.[1,2] As a result of these structural changes, colloidal suspensions can exhibit non-Newtonian behaviors such as shear thinning,[3,4] shear thickening,[5–11] and viscoelasticity.[12,13] As such, developing a relationship between interparticle interactions and suspension-level transport is a crucial goal for understanding many natural systems and soft materials.

Particle interactions in colloidal systems typically result from the local distribution of small molecules, polymers, or ions near the surfaces of the colloids. Particularly, adding non-adsorbing polymer coils to a colloidal suspension induces an entropic depletion force, responsible for a rich variety of phase phenomena including flocculation,[14] liquid-liquid phase separation,[15] and nucleation and crystallization.[16] Established by Asakura, Oosawa (AO), and Vrij,[17,18] depletion forces at equilibrium result from depletants preferentially excluding from the vicinity of the larger colloids to induce an entropic attraction between colloidal pairs that scales with the thermal energy k_BT and the depletant concentration, n_b. Equilibrium-based models of the depletion potential have also been broadly applied to suspensions driven out of thermodynamic equilibrium as an approximation of the interparticle interactions. In biology, AO-type depletion potentials have been proposed as a model for reversible aggregation of red blood cells.[19–21] In synthetic systems, equilibrium depletion potentials are used to predict the rheology of colloid-polymer mixtures[22] and in simulating depletant-induced gelation processes.[23 24–27] The key underlying assumption is that there exists a separation of timescales between the slow rearrangement of large colloidal particles and the rapid equilibration of the small polymeric depletant bath, $\tau_c \gg \tau_b$, such that the depletant distributions behave quasi-statically under any nonequilibrium process which disturbs the colloidal-scale microstructure.

However, when the flow velocity is comparable to the thermal Brownian velocity of the depletants, the depletants no longer assume an equilibrium Boltzmann distribution around the colloids and the classic AO depletion potential is no longer an accurate model for colloidal interactions. For example, Dzubiella and coworkers have shown theoretically that two fixed colloids in a drifting depletant bath exhibit anisotropic, flow-dependent depletion forces,[28] which have also been confirmed by Sriram and Furst through optical trapping experiments.[29] As a separate example, Xu and Choi et al. recently demonstrated that polymer-coated colloids exhibit dynamic pairwise forces which slowly relax over time when colloids are driven towards each other at speeds comparable to polymer surface diffusion.[30] While such nonequilibrium effects are important in dictating the macroscopic

[a] Department of Chemical Engineering, University of California, Santa Barbara, Santa Barbara, CA, USA.
‡ Corresponding author. Email: stakatori@ucsb.edu

† Electronic Supplementary Information (ESI) available: See DOI: 10.1039/cXsm00000x/

behavior of driven suspensions, developing models for out-of-equilibrium particle interactions remains a challenge. Previous work has primarily focused on bath particle organization around fixed colloids, while colloids in a free suspension are able to undergo motion under various forces such as Brownian diffusion and advection.[31,32] It is still unclear how the local polymer distributions and timescales couple to suspension-level processes. We hypothesize that a competition between the depletant timescales τ_b and colloidal process timescales τ_c in nonequilibrium systems ultimately controls the suspension microstructure and rheology.

In this work, we use Smoluchowski theory and Brownian dynamics (BD) simulations to develop a multiscale framework for studying nonequilibrium interactions among colloids driven out of equilibrium. As a specific case study, we focus on the nonlinear microrheology of a bidisperse suspension of colloids and depletants. We show that the nonequilibrium colloidal microstructure and viscosity cannot generally be predicted by a naive application of an AO-type depletion potential. To the best of our knowledge, this work is the first full micro-mechanical consideration of a nonequilibium, multi-phase suspension that does not rely on any standard, equilibrium-based approximations.

The remainder of this paper is organised as follows. In Section 2 we describe the model suspension and use the Smoluchowski framework to derive governing equations for the colloidal microstructure and viscosity. In Section 3 we present our results and analysis. Finally, we discuss the implications of our work in Section 4.

2 Methods

2.1 Model Preliminaries

Our theoretical framework is general to any imposed hydrodynamic flow, but we chose to focus here on a nonlinear microrheology problem to make comparisons with existing work. As depicted in Fig. 1, we consider a 2-dimensional system of two interacting colloidal particles suspended in a bath of smaller, ideal depletant particles in a Newtonian solvent with viscosity η and temperature T. Assuming the polymeric depletant behaves as a random walk chain that can be mapped onto a hard sphere, we choose the particle radii of the colloids and depletants as $d_c = 5\sigma$ and $d_b = 1\sigma$, respectively. We assume that the depletants are ideal and mutually uncorrelated but can interact with the larger colloidal particles. In constant-velocity nonlinear microrheology, we consider the behavior when one colloid particle (the "probe") is driven in the positive-x direction through the suspension at a probe velocity, $\mathbf{U}_1 = U_c\mathbf{e}_x$, while all other particles move through Brownian motion and are quiescent. As the probe is pulled through the suspension, it experiences viscous drag forces from the Newtonian solvent and also from random collisions with suspended particles. Under these effects, the imposed velocity is related to an average force felt by the probe $\langle \mathbf{U}_c \rangle = \mu_p \mathbf{F}_1$ where μ_p is the mobility of the probe. This is contrasted with passive microrheology, where the probe itself undergoes Brownian fluctuations, and with constant-force nonlinear microrheology, where the probe is pulled at a fixed force and moves under a velocity that has been averaged over collisions with all remaining particles.

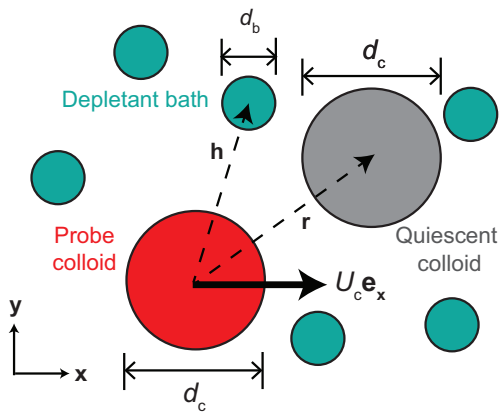

Fig. 1 Schematic of a bidisperse model system depicting one probe colloid (red) and one quiescent colloid (gray) with size d_c suspended in a dilute bath of smaller bath particles (blue) with size d_b. The probe is driven at constant velocity U_c in the positive x-direction. The coordinates (h, r) denote the positions of a depletant and the quiescent colloid relative to the probe, respectively.

Neglecting hydrodynamic interactions, the viscous drag experienced by the depletants, ζ_b, and by the quiescent colloid, ζ_c, is related through a drag parameter, $\alpha = \zeta_c/\zeta_b$. Under the Stokes-Einstein-Sutherland (SES) relation for particle diffusion coefficients, $D_{c,b} = k_B T/\zeta_{c,b}$, the relative drag parameter reduces to a ratio between the particle sizes, $\alpha = d_c/d_b = 5$.[2] To thoroughly explore the relationship between diffusive timescales and microstructure, we consider the general case where the frictional drag coefficients may deviate from the SES relation. For example, if particles are embedded in a more complex environment, such as a hydrogel network, α may additionally depend on parameters such as mesh size and mesh stiffness.[33–36] To reduce the number of parameters, we define a Péclet number $\mathrm{Pe}_c = U_c d_b/D_c$ relating the driving velocity to the speed at which the colloid diffuses in space. In general, the Péclet number Pe indicates the relative importance of external forcing to the thermal, restorative forces of the material. Since there are two particle species in the system, a second Peclet number, $\mathrm{Pe}_b = U_c d_b/D_b$ relates the driving velocity to the speed at which the polymeric depletant diffuses. We note that these two nondimensional quantities are exactly related through the drag parameter, $\mathrm{Pe}_b = \mathrm{Pe}_c/\alpha$.

We now explain the micro-mechanical framework for this bidisperse suspension below.

2.2 Smoluchowski Framework

In colloidal suspensions, the microstructural response to nonequilibrium perturbation determines the rheological response of the material. The time-dependent distribution of particles in a suspension obeys the Smoluchowski equation, which balances fluxes of advection, interparticle forces, and Brownian diffusion.[1,3,13,37–39] We have labeled all quantities with respect to the probe with the subscript $i = 1$, the quiescent colloid with $i = 2$, and the bath depletant with $i = 3$, respectively. The three-particle distribution P_3 of the probe, the quiescent colloid, and a depletant

particle is given by:

$$\frac{\partial P_3}{\partial t} + \nabla \cdot \langle \mathbf{j}_2 - \mathbf{j}_1 \rangle_3 + \nabla_{\mathbf{h}} \cdot \langle \mathbf{j}_3 - \mathbf{j}_1 \rangle_3 = 0. \quad (1)$$

In Eq. 1, $\mathbf{j}_1$ is the probe flux, which is deterministic when driven at constant velocity, $\mathbf{j}_2$ is the flux of the quiescent colloid, and $\mathbf{j}_3$ is the flux of the bath depletant. The brackets $\langle ... \rangle_3$ represent a statistical average over the degrees of freedom of $N-1$ depletant particles. The relative flux of the quiescent colloid $\langle \mathbf{j}_2 - \mathbf{j}_1 \rangle$ is:

$$\langle \mathbf{j}_2 - \mathbf{j}_1 \rangle_3 = -\alpha^{-1} \left[\mathrm{Pe_c} P_3 \mathbf{e}_x + P_3 \nabla (V_{21} + V_{32})/(k_\mathrm{B}T) + \nabla P_3 \right], \quad (2)$$

and the relative flux of the depletant $\langle \mathbf{j}_3 - \mathbf{j}_1 \rangle$ is:

$$\langle \mathbf{j}_3 - \mathbf{j}_1 \rangle_3 = -\alpha^{-1} \mathrm{Pe_c} P_3 \mathbf{e}_x - P_3 \nabla_{\mathbf{h}} (V_{31} + V_{32})/(k_\mathrm{B}T) - \nabla_{\mathbf{h}} P_3. \quad (3)$$

The terms on the right hand side of Eq. 2and Eq. 3 represent contributions from advection due to probe motion, interparticle forces derived from probe-colloid (V_{12}), probe-depletant (V_{13}), and colloid-depletant (V_{23}) pair potentials, and thermal motion, respectively. We have rescaled all distances by the depletant size d_b, energies by the thermal energy $k_\mathrm{B}T$, and time by the Brownian timescale of the depletant particle, $\tau_\mathrm{c}^{\mathrm{Brownian}} = d_\mathrm{b}^2/D_\mathrm{b}$. In general, the Smoluchowski equation for P_3 depends on higher order moments that involve the conditional distributions of the remaining $N-1$ particles. To render the equation tractable, in writing down Eq. 1-3, we have opted for a closure relation which neglects those higher order contributions. A more detailed derivation of these equations from a general Smoluchowski equation is provided in the Supplementary. All derivatives and gradients with respect to the colloidal position are defined as $\nabla \equiv \nabla_{\mathbf{r}}$ for notation simplicity.

The three particle probability may be defined in terms of conditional probabilities, $P_3 = P_1 P_{1|1}(\mathbf{r},t) P_{1|2}(\mathbf{h},t|\mathbf{r})$. Here, $P_{1|1}(\mathbf{r},t)$ is the probability of finding the quiescent colloid at position $\mathbf{r}$ and $P_{1|2}(\mathbf{h},t|\mathbf{r})$ is the probability of finding a depletant particle at $\mathbf{h}$ given that the quiescent colloid is at $\mathbf{r}$. These conditional probabilities are related to physical quantities by $P_{1|1}(\mathbf{r},t) = n_\mathrm{c} g(\mathbf{r},t)$ and $P_{1|2}(\mathbf{h},t|\mathbf{r}) = n_\mathrm{b} \rho(\mathbf{h},t|\mathbf{r})$ where g is the colloidal pair distribution function and ρ is the local depletant structure about the colloidal pair in a particular configuration. We observe that the colloid pair distribution satisfies mass conservation, $g(r) = n_\mathrm{b} \int g(\mathbf{r}) \rho(\mathbf{h}|\mathbf{r}) d\mathbf{h}$. Additionally, because hard particles cannot overlap, Eq.1 satisfies no-flux boundary conditions at hard-disk contact distances, $\mathbf{n}_h \cdot \langle \mathbf{j}_3 - \mathbf{j}_1 \rangle_3 = 0$ at $h = d_\mathrm{cb} = (d_\mathrm{c} + d_\mathrm{b})/2$ and $\mathbf{n}_r \cdot \langle \mathbf{j}_2 - \mathbf{j}_1 \rangle_3 = 0$ at $r = d_\mathrm{c}$. At infinitely large separations, the depletants and colloid are uniformly distributed and uncorrelated, $g, \rho \to 1$ for $r, h \to \infty$.

The integration of Eq. 1 over the last depletant degree of freedom results in a two-body Smoluchowski equation:

$$\nabla \cdot \langle \mathbf{j}_2 - \mathbf{j}_1 \rangle_2 = 0 \quad (4)$$

where the average colloidal flux is:

$$\langle \mathbf{j}_2 - \mathbf{j}_1 \rangle_2 = -\mathrm{Pe_c} \alpha^{-1} \mathbf{e}_\mathbf{x} g - \alpha^{-1} \left[\nabla g + g \nabla V_{12}/(k_\mathrm{B}T) + g n_\mathrm{b} \int \rho \nabla V_{23}/(k_\mathrm{B}T) d\mathbf{h} \right]. \quad (5)$$

The contributions on the RHS of the average colloidal flux are advection, Brownian, colloid-probe interactions, and an average bath-mediated colloid-probe interaction. We observe that Eq. 4- 5 are standard, pair-level equations which have been used extensively and successfully to model distributions of mono-disperse colloidal suspensions. The main focus of our present work is the last term in Eq. 5. In most prior works, ρ is not explicitly solved for and the last term in Eq. 5 is instead approximated by an equilibrium pair potential such as DLVO theory or Asakura-Oosawa depletion interactions even while the system is driven out of equilibrium, as we will briefly describe in the next section.

2.3 Asakura-Oosawa (AO) Model

The Smoluchowski equation we have previously laid out constitutes a framework in which the bath flux is explicitly considered when deriving the suspension microstructure. The microstructural deformation becomes a function of both the nonequilibrium driving strength and the relative rate of diffusive transport between the colloid and the bath, $g(\mathbf{r},t;\mathrm{Pe_c},\alpha)$. To validate our framework and demonstrate its advantages in nonequilibrium settings, we will compare our approach to a conventional treatment which uses an equilibrium depletion potential. In this treatment, rather than considering the nonequilibrated local bath distribution ρ, we impose a quasi-static, attractive pair potential between the colloid and the probe, such that their relative motion is governed by a two-body Smoluchowski equation:

$$\frac{dg}{dt} + \nabla \cdot \langle \mathbf{j}_2 - \mathbf{j}_1 \rangle_2 = 0 \quad (6)$$

where the relative translational flux is given by:

$$\langle \mathbf{j}_2 - \mathbf{j}_1 \rangle = -\mathrm{Pe_c} g \mathbf{e}_x - g \nabla V_\mathrm{AO}/(k_\mathrm{B}T) - \nabla g. \quad (7)$$

Observe that Eq. 7 is identical to Eq. 5 if the pairwise forces obtained from the equilibrium approximations satisfy $\nabla V_\mathrm{AO} = \nabla V_{12}/(k_\mathrm{B}T) + n_\mathrm{b} \int \rho \nabla V_{23}/(k_\mathrm{B}T) d\mathbf{h}$. Physically, this means that the AO potential is equivalent to a local bath distribution which instantaneously equilibrates about the two larger colloids.

At equilibrium, the structure of a homogeneous mixture gives the effective depletion potential, which in two dimensions is given by:[40,41]

$$V_\mathrm{AO}/k_\mathrm{B}T = -n_\mathrm{b} d_\mathrm{b}^2 \frac{(1+a)^2}{2} \left[\cos^{-1}\left(\frac{1}{1+a} \frac{r}{d_\mathrm{b}} \right) - \left(\frac{1}{1+a} \frac{r}{d_\mathrm{b}} \right) \sqrt{1 - \left(\frac{1}{1+a} \frac{r}{d_\mathrm{b}} \right)^2} \right] \quad (8)$$

where $a = d_\mathrm{c}/d_\mathrm{b}$. Similar to Eq. 1, Eq.6 satisfies no-flux boundary conditions $\mathbf{n} \cdot \langle \mathbf{j}_2 - \mathbf{j}_1 \rangle_3 = 0$ at contact $r = d_\mathrm{c}$ and uniform distributions far away, $g \to 1$ for $r \to \infty$. Under Eq. 6- 7, the microstructural deformations do not depend on depletant transport and are purely functions of the probe driving strength, $g(\mathbf{r},t;\mathrm{Pe_c})$. This simple theory serves as a check of our framework at equilibrium, and we will now consider its utility out of equilibrium.

2.4 Regular Perturbation

In general, Eqs. 1- 3 are difficult to evaluate numerically because the equation depends on both the bath and colloidal degrees of freedom. However, if the depletant diffuses much faster than the colloid in the suspension, then the drag parameter α is much greater than 1. In this limit, we can solve Eq. 1 using a regular perturbation expansion $\rho \approx \rho_0 + \alpha^{-1}\rho_1 + \mathscr{O}(\alpha^{-2})$ and $g \approx g_0 + \alpha^{-1}g_1 + \mathscr{O}(\alpha^{-2})$ (see Supplemental). This is analogous to a multiple-timescale approach, where the effective depletion force at equilibrium may be obtained by expanding the time variable in terms of the "fast" timescale of the depletants.[42–44] Physically, the regular perturbation implies that the probe is driven at strengths comparable to thermal fluctuations of the depletant (i.e. the linear response limit). Note that the driving strength is not necessarily weak relative to colloidal diffusion, which allows us to measure the nonlinear microrheology of the colloidal suspension.

Using regular perturbation, we evaluate Eq. 1- 3 at steady state and find that the leading order depletant distribution is a Boltzmann distribution $\rho_0 \sim e^{-V_{23}-V_{13}}$, consistent with our assumption that the fastest timescale in the system is depletant diffusion. The leading order colloidal distribution obeys:

$$\nabla\cdot\left[\mathrm{Pe_c} g_0 \mathbf{e_x} + \nabla g_0 + g_0\nabla V_{12}/(k_\mathrm{B}T) - g_0 n_\mathrm{c}\int \rho_0 \nabla V_{23}/(k_\mathrm{B}T) d\mathbf{h}\right] = 0. \tag{9}$$

The first three terms on the left-hand side of Eq. 9 are identical to Squires and Brady for a monodisperse bath,[39] while the last term is a potential of mean force between the probe and colloid due to the presence of depletants. We have further derived the governing equations for the $\mathscr{O}(\alpha^{-1})$ contribution in the Supplementary. All equations are numerically evaluated for an arbitrarily large 2-dimensional area using FreeFEM++, an open-source finite element package.[45]

2.5 Viscosity Calculation

When driven at a constant velocity $\mathbf{U}_\mathrm{c}$ through the suspension, the probe experiences both a Newtonian drag due to the solvent and an additional, effective drag due to interactions with other particles. For arbitrary pairwise interactions, it may be shown that the average force felt by the probe is given by:

$$\langle \mathbf{F}_1 \rangle = \frac{\mathbf{U}_\mathrm{c}}{3\pi\eta d_\mathrm{c}} + n_\mathrm{c} k_\mathrm{B}T \int g \nabla V_{21} d\mathbf{r} + n_\mathrm{c} n_\mathrm{b} k_\mathrm{B}T \int g \int \rho \nabla_\mathbf{h} V_{31} d\mathbf{h} d\mathbf{r}. \tag{10}$$

The additional viscosity due to particle interactions may be related to Stokesian-type drag, $\langle \mathbf{F}_1 \rangle = 3\pi\eta_\mathrm{eff} d_\mathrm{c} \mathbf{U}_\mathrm{c}$. One may compute the effective viscosity increment $\Delta\eta_\mathrm{eff} = \eta_\mathrm{eff} - \eta$, which is given by:

$$\frac{\Delta\eta_\mathrm{eff}}{\eta} = \frac{n_\mathrm{c} k_\mathrm{B}T}{3\pi\eta d_\mathrm{c} U_\mathrm{c}} \int g \nabla V_{21} d\mathbf{r} + \frac{n_\mathrm{c} n_\mathrm{b} k_\mathrm{B}T}{3\pi\eta d_\mathrm{c} U_\mathrm{c}} \int g \int \rho \nabla_\mathbf{h} V_{31} d\mathbf{h} d\mathbf{r}. \tag{11}$$

The first term on the right-hand side of Eq. 11 exactly matches the result arrived at by Squires and Brady for a monodisperse suspension, except that, in this case, the pair distribution g is modified by depletant motion.[39] The second term contributes an $\mathscr{O}(n_\mathrm{b})$ effect and accounts for contributions arising from hard-disk collisions with the depletant particles. One may rationalize this depletant concentration dependence by considering that the AO interaction potential also scales with n_b. We note that our multiscale model naturally reduces to the AO pair interaction in the limit of rapidly-equilibrating depletants.

In the next section, we detail our simulation protocol and our choice of particle pair interactions.

2.6 Brownian Dynamics Simulations

To validate our Smoluchowski theory, we perform 2-dimensional BD simulations of the aforementioned viscous suspension of two colloidal particles suspended in a bath of smaller depletants. In the simulation, one probe colloid moves deterministically with constant velocity $U_\mathrm{c}\mathbf{e}_x$ such that in the reference frame of the probe, the quiescent colloid and depletants follow the overdamped Langevin equation of motion:

$$\frac{\Delta r_i}{\Delta t} = \zeta^*_\mathrm{c,b}\Big(\underbrace{\nabla_i V^\mathrm{tot}}_{\text{interactions}} + \underbrace{\mathbf{F}^\mathrm{B}_i}_{\text{Brownian}}\Big) - \underbrace{\mathrm{Pe_b}\mathbf{e}_x}_{\text{advection}} \tag{12}$$

where $\gamma^*_\mathrm{c,b} = \zeta_\mathrm{c,b}/\zeta_\mathrm{c}$ is the non-dimensional drag of the corresponding depletant or colloid. Here, we have nondimensionalized time by the diffusive timescale of the depletants $d_\mathrm{b}^2/D_\mathrm{b}$, positions by the depletant size d_b, and all forces by $k_\mathrm{B}T/d_\mathrm{b}$. The implicit solvent induces a stochastic force $\mathbf{F}^\mathrm{B}_i$ satisfying zero mean and variance consistent with the fluctuation-dissipation theorem. In all simulations, we have chosen a time step, $\Delta t = 10^{-4}$.

All interparticle forces are derived from a global potential:

$$V^\mathrm{tot} = \sum_\mathrm{i}\sum_\mathrm{j} V_\mathrm{ij}(r_\mathrm{ij}) \tag{13}$$

where V_ij is the pairwise potential between particles i and j at separation r_ij. As mentioned earlier, we neglect any depletant-depletant interactions and assume that they are ideal. To model the short-ranged repulsion between particles, we impose the Weeks-Chandler-Anderson (WCA) potential between all remaining particles pairs:[46]

$$V_{ij}(r_{ij}) = \begin{cases} 4\varepsilon\left[\left(\frac{d}{r}\right)^{12} - \left(\frac{d}{r}\right)^{6}\right] + \varepsilon & (r \le 2^{\frac{1}{6}}d) \\ 0 & (r > 2^{\frac{1}{6}}d) \end{cases} \tag{14}$$

where d is the hard-disk contact distance, either d_c for probe-colloid pair interactions V_{12} or d_cb for colloid-depletant and probe-depletant interactions ($V_{12}, V_{2j\neq 1,2}$), and ε is set as the thermal energy scale.

From the simulations, we compute the average drag force on the probe due to collisions with the quiescent colloid ($i = 2$) and with the depletants ($i = 3, \ldots, N+2$),

$$\langle \mathbf{F}_1 \rangle = -\frac{1}{2}\sum_{i=2}^{N+2} \nabla_i \left(\frac{V^\mathrm{tot}}{k_\mathrm{B}T}\right). \tag{15}$$

which is related to the effective viscosity, as shown earlier.

All simulations are performed in a periodic box with dimensions $L_x \times L_y$. For weak driving ($\mathrm{Pe_c} \le 1$), we choose $L_x = 22\sigma$

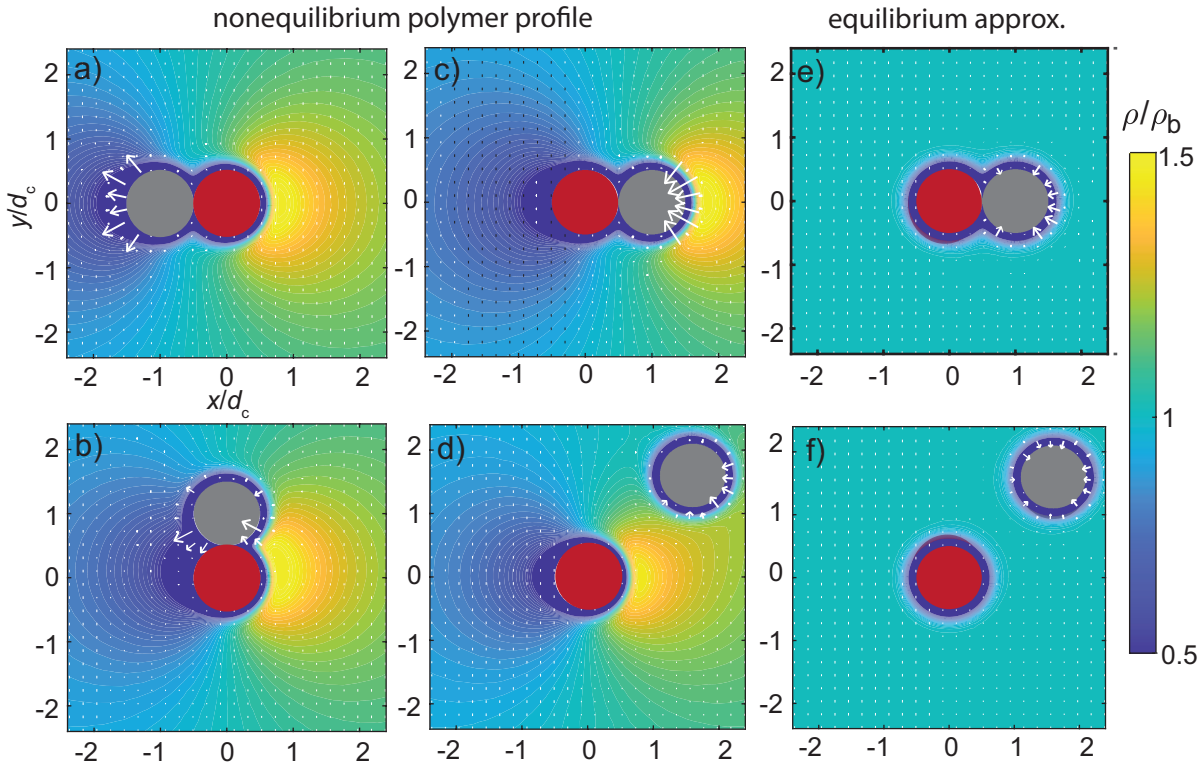

Fig. 2 Local depletant density transmits an effective nonequilibrium force between the quiescent colloid and the driven probe. Perturbation solutions of Eq. 1 for the steady-state conditional depletant density $\rho(\mathrm{h}|\mathrm{r})$ are shown given that the quiescent colloid (gray) is spatially fixed at a position (a) behind, (b) alongside, (c) in front of, and (d) far from the probe (red). The quiescent colloid disrupts the depletant dipole organization when in vicinity of the probe. White arrows indicate the the local, nonequilibrium force field on the quiescent colloid, weighted by the local polymer density, $\rho\nabla_{\mathrm{h}}V^{\mathrm{tot}}$. The drag parameter is $\alpha=\zeta_{\mathrm{c}}/\zeta_{\mathrm{d}}=5$ and driving force is $\mathrm{Pe}_{\mathrm{c}}=10$. For contrast, equilibrium distributions ρ_{eq} are shown when the quiescent colloid is (e) close to and (f) far from the probe, where excluded area overlap results in a classic 2D depletion force. Comparison of panels (e)-(f) with panels (c)-(d) show dramatic differences in the distribution of the depletants around the colloids, demonstrating the inaccuracies of applying the equilibrium AO depletion potential in nonequilibrium processes.

and $L_y=18\sigma$. Under moderate driving ($\mathrm{Pe}_{\mathrm{c}}>1$), a trailing wake begins to form behind the microrheological probe. Therefore, we have increased the x-dimension in those simulations to $L_x=180\sigma$ to ensure that results are not biased by finite size effects. Based on box dimensions, we have chosen the number of bath particles to maintain a high bulk density of ideal depletants, $n_{\mathrm{b}}=0.63d_{\mathrm{b}}^{-2}$. To obtain sufficient statistics, we simulate 30-100 independent realizations and sample statistics for up to $10,000$ depletant Brownian timescales and $200-2000$ colloidal Brownian timescales to ensure steady state spatial distributions. All simulations are performed using HOOMD-blue, a GPU-accelerated simulation package.[47]

3 Results

3.1 Nonequilibrium Depletant Microstructure

To understand how the depletant bath modifies colloidal interactions out of equilibrium, we first consider the micro-scale depletant structure around the colloidal pair. For an ideal, monodisperse suspension, it is well known that bath particles at steady state adopt a symmetric diffusive dipole, $\rho(h,\theta)=1+\mathrm{Pe}_{\mathrm{b}}\cos(\theta)/(2h^2)$, where bath particles accumulate in front of the probe and deplete from the back.[39] In Fig. 2, we solve Eq. 1 using the regular perturbation approach and present contour plots of the local depletant distribution ρ at a moderate driving strength $\mathrm{Pe}_{\mathrm{c}}=1$ and $\alpha=d_{\mathrm{c}}/d_{\mathrm{b}}=5$, corresponding to the SES limit. In the presence of the second quiescent colloid, the depletant structure exhibit significant deviations from the monodisperse limit when the colloid is in the viscinity of the probe. When the quiescent colloid is upstream of the probe (where it spends a nontrivial amount of time), the depletants accumulate about the quiescent colloid (Fig. 2c). On the other hand, when the quiescent colloid is located downstream, depletants exclude behind the quiescent colloid (Fig. 2a). In both cases, the quiescent colloid effectively "shields" the probe, mitigating the retardation felt by the probe from collisions with the bath. When colloids are separated far apart (Fig. 2d), the dipole is recovered and the depletant density around the colloid is generally undisturbed. These near-field deviations have not been previously predicted by equilibrium-based assumptions such as dynamic superpositioning approximation (DSA), which do not preserve the internal force transmissions between the particles[48].

In Fig. 2e-f, we verify our theory at equilibrium by showing that the depletant microstructure follows a Boltzmann-like distribution, where the depletant density is unity except inside the excluded volume shells around each colloid. While the net depletion force at equilibrium points along the centers-of-mass axis between the probe and the colloid, the nonequilibrium depletion

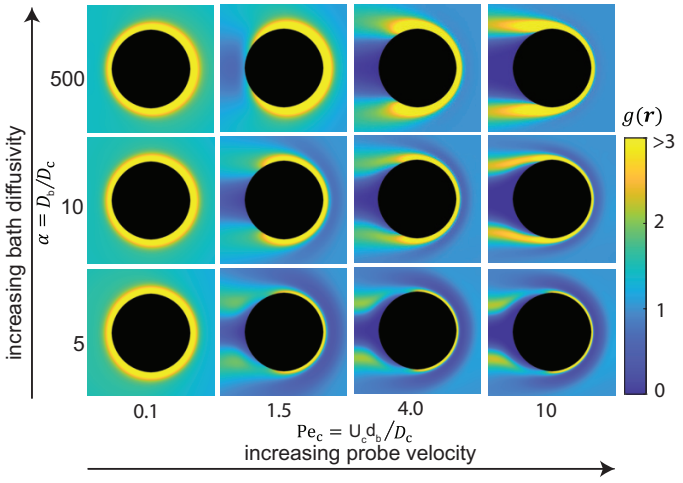

Fig. 3 Competition between depletant and colloidal timescales governs the steady-state colloidal microstructure out of equilibrium. Contour plots for the colloidal pair distribution $g(r)$, obtained from numerically solving the steady-state solution to Eq. 1, are shown for a range of depletant diffusivities α and probe velocities Pe_c. The colloidal distribution at low-Pe_c is uniformly isotropic while a boundary layer and trailing wake develops at higher Pe_c. An upstream ring of depleted density develops at higher Pe_c and low α due to nonequilibrium depletant interactions.

force is generally anisotropic and acts along the direction of probe motion (Fig. 2a-d). Given their strength and anisotropy, we expect that these nonequilibrium forces will significantly impact the colloidal microstructure. Our results demonstrate that the distribution of depletants is no longer Boltzmann in the presence of forcing, and that the nonequilibrium distributions of the depletants play a key role in dictating the effective forces on the colloids. As we discuss in further detail below, the equilibrium AO potential cannot be used in general to accurately predict the colloidal distributions driven out of equilibrium.

3.2 Colloidal Microstructure

Given the local, flow-dependent organization of depletant particles, we now consider how the colloidal scale microstructure is modified by these nonequilibrium depletion interactions. In Fig. 3, we show contour plots for the steady colloidal pair distribution function $g(r)$ for a range of depletant diffusivities α and probe driving strengths Pe_c. Surprisingly, we find that the moderate to high Pe behavior is sensitive to the diffusivity of the bath. In a monodisperse suspension under strong shear, one expects microstructural deformations to collapse to a convection-diffusion boundary layer of width $d_c Pe_c^{-1}$ at sufficiently high Pe_c. For a bidisperse suspension, while the boundary layer is recovered in the limit of very diffusive depletants, an upstream ring of essentially no colloidal density with width d_b appears for lower values of α. This is indicative of repulsive interactions between the colloid and probe beyond their hard sphere-like interaction. In a previous study, this repulsion has been attributed to the interactions facilitated by depletants, but the mechanism by how this occurred was not clear.[48] When the probe velocity is comparable to the depletant timescale, the depletant-mediated nonequilibrium force tends to push the colloid away from the leading probe front and towards the back. (Supplementary Fig. 1) Due to the local dipolar distribution of depletants, this nonequilibrium depletion force tends to be stronger and longer-ranged than the equilibrium force, which disappears once $|\mathbf{r}| > d_c + d_b$. Additionally, we observe that the low-Pe_c behavior is isotropically enriched, indicative of an isotropic attractive depletion potential.

To quantitatively consider the colloidal microstructure at moderate Pe_c, we perform BD simulations and average over a representative cross-section of $g(r)$ along the upstream direction. In Fig. 4a, we show both the equilibrium distribution and a nonequilibrium distribution at a driving velocity $Pe_c = 1$ for low ($\alpha = 5$) and high ($\alpha = 50$) depletant diffusivities. We plot our BD simulations, theoretical solutions to Eq. 1-Eq. 3, and results using the equilibrium approximation with an AO depletion potential (Eq. 6-Eq. 8). Overall, BD simulations show good agreement with the theoretical solutions. The equilibrium $g(r)$ enriches at contact $r/d_c = 1$ due to AO-type depletion interactions and is independent of α. This is consistent with the intuition that the equilibrium distribution is only dependent on the potential energy landscape and is insensitive to transport properties such as diffusivity. We note that the hard sphere contact distance limits our multi-scale solutions to $r/d_c \geq 1$.

Interestingly, two distinct characteristics arise when the probe is driven. First, when depletants diffuse much faster than the colloid ($\alpha = 50$), the peak in $g(r)$ at $r/d_c = 1$ increases by roughly 60% due to advection-driven accumulation along the upstream direction. On the other hand, when the depletants are diffusing at similar speeds as the colloidal particle ($\alpha = 5$), the enrichment at contact is significantly dampened. The AO theory accurately predicts the former but has no way of accounting for the latter. We rationalize that because the AO model assumes a quasi-equilibrium distribution of bath particles, it therefore relies on having a large separation of timescales, or large α. Secondly, while one would expect uniform attraction (i.e. $g(r) \geq 1$ for all r) for depletion interactions, we find that the suspension shows a slight decrease near $r/d_c \sim 1.2$ when the bath is less diffusive. This decrease corresponds to the repulsive ring that was qualitatively observed in Fig. 3. AO-theory fails to predict the repulsive behavior, which must be purely a nonequilibrium effect. We verified that deviations of the theoretical results from simulations at $r \geq 1.2$ are attributed to indirect correlations between the ideal depletants, which exist at high number densities in our simulations. We note that this depletant-mediated repulsion is distinct from the pairwise repulsion in colloidal systems coated with interacting, end-tethered polymer brush layers[14]. While the polymer brush system results in a entropic repulsion at equilibrium, the depletant-mediated pair interaction is purely attractive at equilibrium and the repulsion is a nonequilibrium effect associated with the intrinsic depletant timescale.

In Fig. 4b, we propose one mechanism by which the competition of diffusive timescales helps to facilitate this short-range attraction and longer-range repulsion. When the probe is driven at moderate strengths, the particles in suspension accumulate (i.e. spend a non-negligible amount of time) at the upstream surface of the probe. When the colloid is separated from the probe by a layer of smaller bath particles, a more diffusive bath is less perturbed

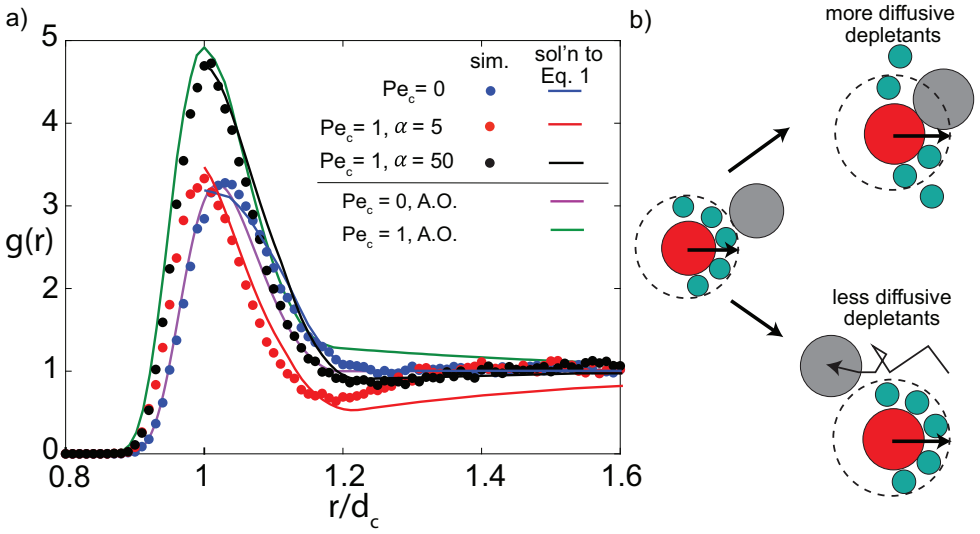

Fig. 4 Depletant diffusivity modulates a short-range attraction and longer-range repulsion between colloidal pairs out of equilibrium. (a) The steady colloidal pair distribution function $g(r)$ upstream of the microrheological probe is plotted as a function of the center-center separation between the colloids. Filled markers are BD simulations for the equilibrium suspension (blue) and the nonequilibrium suspension ($\mathrm{Pe_c} = 1$) in a less diffusive (red) and more diffusive (black) depletant bath. Solid curves are solutions to Eq. 1. The Asakura-Oosawa approximation is also plotted for $\mathrm{Pe}_c = 0$ (purple) and $\mathrm{Pe}_c = 1$ (green). Numerical solutions are truncated at Eq. 1 $\mathrm{r/d}_c$ where we have imposed a no flux condition. (b) Proposed mechanism of how depletant diffusivity modulates colloidal microstructure. Given their spatial diffusivity, depletants either quickly relax and move away to allow colloids to come into contact (top) or form a boundary layer that shields the probe (bottom).

by flow and allows the colloid to make contact with the probe by diffusing away from the interstitial region. As such, an AO-type depletion attraction is maintained because depletants are able to reach local equilibrium. However, when the bath depletants diffuse comparably as fast as the colloid, the depletants accumulate more strongly upstream and therefore requires more work for the colloid to penetrate. In this case, the quiescent colloid effectively "sees" a larger probe of diameter $d_\mathrm{c} + d_\mathrm{b}$.

Finally, using our theoretical framework, we have derived a nonequilibrium potential of mean force between colloidal particles which may be more practical for many-body systems under assumptions of weak driving forces (see Supplemental for detailed derivation). Unlike the equilibrium pairwise interaction V_eq which is equivalent to AO and is purely isotropic, the nonequilibrium pair interaction V_neq depends specifically on the nonequilibrium protocol and may also depend on the relative angle of separation. In Fig. 5, we show the nonequilibrium and equilibrium pair interactions along the leading front of the probe for $\alpha = 10$ and colloid Péclet Number $Pe_c = 0.1$. In agreement with Fig. 4, V_neq contributes a repulsive barrier peaked at $r/d_\mathrm{c} = 1.2 = 1 + d_\mathrm{b}/d_\mathrm{c}$, corresponding exactly to the hard-sphere contact distance between two colloids plus the diameter of the depletant particle. This further supports our mechanism that depletants help to shield the probe from the quiescent colloid along the leading front. Additionally, this repulsive potential decays slowly due to the long-ranged, dipolar perturbation to the local depletant structure. Finally, because the equilibrium depletion interaction is purely attractive but limited to $r/d_\mathrm{c} < 1.2$, the net pair interaction demonstrates short-ranged attraction for $r/d_\mathrm{c} < 1.2$ and long-ranged repulsion at $r/d_\mathrm{c} > 1.2$.

3.3 Microviscosity

Microstructural deformations about the probe are of central importance to the rheology of the suspension. In this section, we will study how the microviscosity responds to the competition between various relaxation timescales in our system. We first consider the depletant contribution to the microviscosity by isolating the second term on the right-hand side of Eq. 11, $\Delta\eta_\mathrm{b}/\eta = k_\mathrm{B}T(3n_\mathrm{c}n_\mathrm{b}\pi\eta d_\mathrm{c}U_\mathrm{c})^{-1}\int g\int\nabla_\mathbf{h}V_{31}d\mathbf{h}d\mathbf{r}$ which accounts for the direct interactions between the probe and the depletant. Notice that this term has been normalized by n_c and n_b since it depends on the depletant distribution in the presence of the two colloids. When considering depletant viscosity contributions, the depletant Péclet number, $\mathrm{Pe_b}$, is the relevant nondimensional quantity that measures the driving force relative to depletant Brownian relaxation.

In Fig. 6, we plot $\Delta\eta_\mathrm{b}/\eta$ as a function of $\mathrm{Pe_b}$ for three different depletant ratios. Interestingly, we observe that the depletant microviscosity contribution increases at weak driving and is sensitive to α. When the depletants relax much faster than the colloids ($\alpha = 50$), the probe experiences a lower drag at low shear rates ($\mathrm{Pe_b} \ll 1$), approaching a linear-response plateau at $\mathrm{Pe_b} \to 0$. As probe velocity increases, the viscosity rises to a maximum before monotonically shear-thinning at moderate to high $\mathrm{Pe_b}$. This is markedly different from the typical shear-thinning behavior of hard sphere suspensions. We offer one explanation for this mild shear thickening effect. When α is large, perturbations to the colloidal structure relax much slower and $g(r)$ adopts a boundary layer of $\mathscr{O}(\mathrm{Pe_c})$ with a width of $\mathscr{O}(\mathrm{Pe_c})$.[39] The accumulation of the colloid upstream of the probe prohibits depletants from contacting the probe, as demonstrated earlier in Fig. 2c, and reduces $\Delta\eta_\mathrm{b}/\eta$ at low $\mathrm{Pe_b}$. As $\mathrm{Pe_b}$ increases, the colloid is decreas-

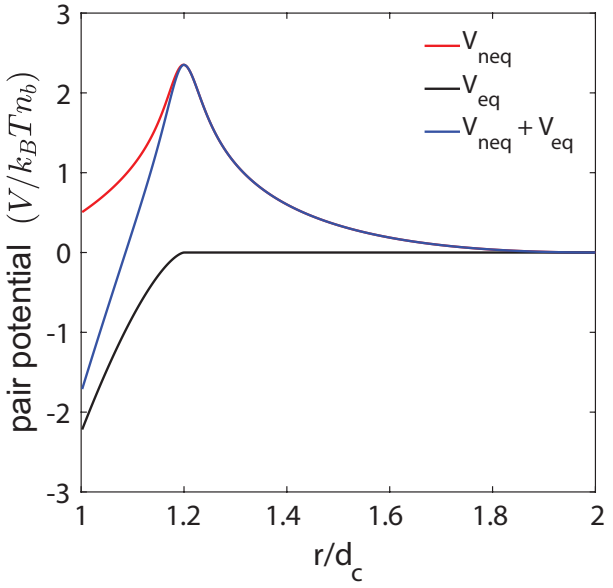

Fig. 5 Nonequilibrium, depletant-mediated interaction potential between colloidal particles. The nonequilibrium pair potential V_{neq}(red), Asakura-Oosawa potential V_{eq} (black), and the net pair interaction (blue) are plotted for large diffusivity ratio $\alpha = 10$ and small colloid Péclet Number $Pe_c = 0.1$.

ingly able to screen out the depletants, thereby leading to an increase in the depletant contribution to the microviscosity. On the other hand, when $\alpha = 5$, $\mathrm{Pe_b}$ is comparable to $\mathrm{Pe_c}$, the viscosity remains relatively flat because both colloids and depletants relax on similar timescales. At moderate to high shear, all cases shear thin. Predicting this limit requires solving the coupled set of Eq. 1- 3 without using regular perturbation, which can only predict a diffusive dipole. Numerical evaluation of those equations are challenging as they require accounting for both colloidal and depletant degrees of freedom simultaneously. Although we do not have a theoretical prediction in this limit, we speculate that the shear thinning behavior is likely similar to that of a monodisperse suspension. At high $\mathrm{Pe_c}$, we observe a prolonged shear decay towards zero in the simulations, which has been previously observed. This shear thinning has been attributed to the inaccuracy of the continuous WCA pair potential in approximating hard spheres in the limit of high probe velocity.[48]. For hard sphere suspensions, it has been previously found that the high shear viscosity flattens toward a finite value as particles accumulate within a convection-diffusion boundary layer of width $\mathrm{Pe_c^{-1}}$, within which the accumulation grows as $O(\mathrm{Pe_c})$.[39].

Finally, we consider the colloidal contribution to the microviscosity by defining $\Delta\eta_c/\eta = k_{BT}(3n_c\pi\eta d_c U_c)^{-1}\int g\nabla V_{21}d\mathbf{r}$ from Eq. 11. In Fig. 7, we plot $\Delta\eta_c/\eta$ as a function of the the colloidal Péclet number, $\mathrm{Pe_c}$ for three different drag ratios. Here, we observe a shear thinning behavior throughout and a small increase in the linear response viscosity for decreasing depletant diffusivity. This is consistent with the intuition that reducing bath diffusivity also increases the relaxation time of the colloid and therefore increases the work required to distort the colloidal microstructure. At higher driving strengths, both theory and simulations indicate a shear thinning behavior, which is commonly observed in monodisperse hard-sphere suspensions without hydrodynamic interactions or contact friction. BD simulations at weak driving suffer strongly from thermal noise and are omitted for clarity.

When both contributions are combined, the overall viscosity of the suspension remains shear thinning despite the mild shear-thickening effect of the bath. However, caution should be taken when directly comparing Fig. 6- 7 for two reasons. First, the x-axis of Fig. 7 is offset from Fig. 6 by a factor of α due to the definition of the Péclet numbers, $\mathrm{Pe_c} = \alpha\mathrm{Pe_b}$. Second, $\Delta\eta_b/\eta$ is normalized by the bath density while $\Delta\eta_c/\eta$, which also contains contributions from the depletants, is not. Therefore, while the viscosity is seemingly dominated by the colloid, in reality the depletants indirectly influence $g(r)$, and $\Delta\eta_c/\eta$ become a weaker contribution once n_b has been scaled out. Finally, for a fixed depletant area fraction $\phi_b = n_b\pi(d_b/2)^2$, we observed similar qualitative features and note that the microviscosity contributions generally decrease as depletant size increases. (Supplementary Fig. 2) Because the depletant number density n_b must decrease to maintain a constant area fraction, both the equilibrium and nonequilibrium depletant interactions will weaken. Therefore, we hypothesize our analysis holds in the limit of small depletants which are present in high concentration.

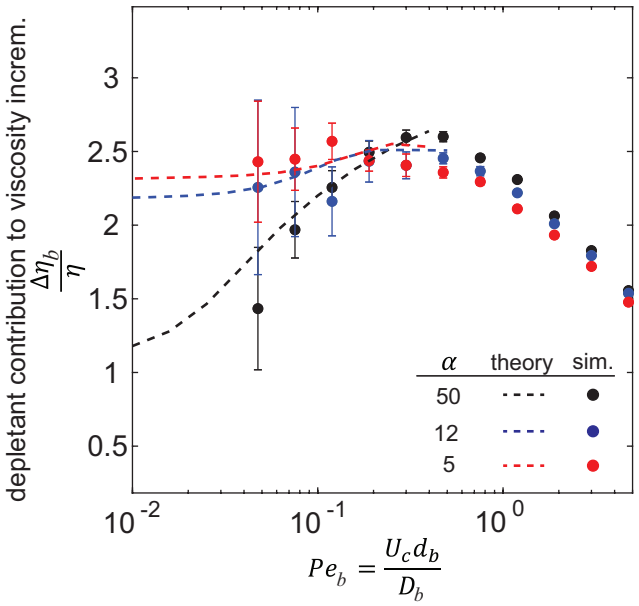

Fig. 6 Viscosity contribution from depletant bath mildly shear thickens at lower shear and shear thins at higher shear. The depletant bath viscosity is plotted as a function of the depletant Péclet number Pe_b for a varying drag ratios of $\alpha = 5$ (red), $\alpha = 12$ (blue), and $\alpha = 50$ (black). Theory predictions from Eqs. 1-3 are only shown for $\mathrm{Pe_b} \leq 0.2$, when the regular perturbation expansion is valid.

4 Discussion

Understanding the material properties of multicomponent suspensions is important for many applications. In this work, we have developed a framework that accurately predicts the structure and microrheology of a bidisperse suspension of colloids and

depletants. We found that the colloidal microstructure is generally sensitive to the bath diffusion timescale and that equilibrium-based approximations toward a depletion pair potential is only reliable in certain limits. While we focus our case study on a dilute suspension with at most pairwise interactions, in denser systems one may opte to apply a mean-field treatment. For a hard sphere suspension, one may incorporate the mean field external potential, which is derived based on the free energy of the system and depends on higher order virial coefficients, into Eq. 1 to account for density effects.[40].

We also qualify our results by observing that beyond a certain flow strength, the polymer may undergo a coil to stretch transition, resulting in stresses that grow nonlinearly with the flow rate.[49] When the deformation time exceeds that of the internal relaxation time of the depletant polymer chain, polymers no longer adopt a random-walk chain and can become elastically stretched. In such cases, the polymeric bath may be better treated as a continuous, viscoelastic fluid instead of hard sphere particles. Previous works have used well-established models such as Giselkus or Oldroyd-B to describe the fluid suspension.[50–52] In such cases, the fluid disturbances due to the particles alone may give rise to shear thickening effects, in the absence of hydrodynamic interactions or frictional effects.[52] In Brownian Dynamics simulations, one could explicitly model internal chain dynamics by representing the polymer as a Kremer-Grest bead spring model.[53] We leave the detailed analysis of such systems to future work.

Although we have not accounted for hydrodynamic interactions, fluid effects play an important role in modifying the rheology and microstructure of colloidal suspensions.[3,4] Our theory may accommodate near-field hydrodynamic functions as a first step towards including fluid-mediated interactions. Additionally, effects such as roughness and friction between particle surfaces may contribute to shear thickening at higher flow strengths.[8–11] We note that our simulations, which measures correlated motion between the probe and anther colloid in a depletant bath, bear similarities with multiparticle microrheology techniques, where the relative motion of multiple probes allows the measurement of collective drift or characterization of material heterogeneities.[54,55]

We conclude with a discussion of the potential applications of our model. Although we have provided the simplest case of depletion interactions facilitated by repulsive, hard disks, future work may look into other types of small particles such as ahesive colloids coated by single-stranded DNA[56–58] or particles stabilized by electrostatic interactions.[14] Furthermore, AO or DLVO potentials are commonly used to model colloidal systems that undergo kinetic arrest and gelation.[24,26,27,59–62] The micro-mechanism we have identified in this work may shed light on the limited applicability of static pair interactions in these nonequilibrium systems. Our framework may also be used to predict other material properties. For example, one may measure viscoelasticity by performing oscillatory shear rheology,[63–65] for which a microscopic theory that accurately predicts the unsteady microstructure and the material moduli of multicomponent suspensions is still lacking. Finally, understanding the interplay between various relaxation timescales in systems of colloidal scale is broadly relevant for a variety of biological systems, including deformable particles[66] and biological cell surfaces where proteins laterally rearrange cell-cell contact.[67]

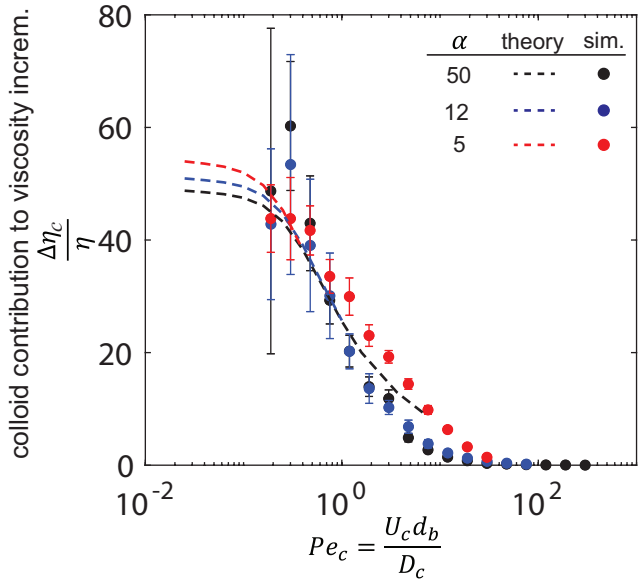

Fig. 7 Viscosity contribution from quiescent colloid shear thins. The viscosity due to interactions with the quiescent colloid is plotted as a function of the colloidal Péclet number Pe_c for three drag ratios: $\alpha = 5$ (red), $\alpha = 12$ (blue), and $\alpha = 50$ (black). Theory predictions from Eqs. 1-3 are only shown for $Pe_c \leq \alpha$, when the regular perturbation expansion is valid.

Author Contributions

Both authors conceived of the study and designed research; Y.X. performed simulations and numerical calculations; S.C.T. supervised the study; and both authors wrote the paper.

Conflicts of interest

There are no conflicts of interest to declare.

Acknowledgements

We would like to thank Glenn Fredrickson and Todd Squires for valuable discussions and feedback. This material is based upon work supported by the Air Force Office of Scientific Research under award number FA9550-21-1-0287. Y.X. acknowledges support from the Dow Discovery Fellowship at UC Santa Barbara. S.C.T. is supported by the Packard Fellowship in Science and Engineering. Acknowledgment is made to the Donors of the American Chemical Society Petroleum Research Fund for partial support of this research. Use was made of computational facilities purchased with funds from the National Science Foundation (OAC-1925717) and administered by the Center for Scientific Computing (MRSEC; NSF DMR 2308708) at UC Santa Barbara.

Notes and references

1 J. Mewis and N. J. Wagner, *Colloidal Suspension Rheology*, Cambridge University Press, 2011.

2 É. Guazzelli, J. F. Morris and S. Pic, *A Physical Introduction to Suspension Dynamics*, Cambridge University Press, 2011.

3 J. Bergenholtz, J. F. Brady and M. Vicic, *Journal of Fluid Mechanics*, 2002, **456**, 239–275.

4 G. K. Batchelor, *Journal of Fluid Mechanics*, 1976, **74**, 1–29.

5 J. Bender and N. J. Wagner, *Journal of Rheology*, 1996, **40**, 899–916.

6 J. R. Melrose and R. C. Ball, *Journal of Rheology*, 2004, **48**, 937–960.

7 J. F. Brady and G. Bossis, *Journal of Fluid Mechanics*, 1985, **155**, 105.

8 R. Mari, R. Seto, J. F. Morris and M. M. Denn, *Journal of Rheology*, 2014, **58**, 1693–1724.

9 R. Mari, R. Seto, J. F. Morris and M. M. Denn, *Proceedings of the National Academy of Sciences of the United States of America*, 2015, **112**, 15326–15330.

10 N. Y. C. Lin, B. M. Guy, M. Hermes, C. Ness, J. Sun, W. C. K. Poon and I. Cohen, *Phys. Rev. Lett.*, 2015, **115**, 228304.

11 S. Pednekar, J. Chun and J. F. Morris, *Soft Matter*, 2017, **13**, 1773–1779.

12 R. A. Lionberger and W. B. Russsel, *J. Rheol.*, 1994, **38**, 1885–1908.

13 A. S. Khair and J. F. Brady, *Journal of Rheology*, 2005, **49**, 1449–1481.

14 W. B. Russel, D. A. Saville and W. R. Schowalter, *Colloidal Dispersions*, Cambridge University Press, 1989.

15 S. M. Ilett, A. Orrock, W. C. K. Poon and P. N. Pusey, *Physical Review E*, 1995, **51**, 1344–1352.

16 A. A. Louis, R. Finken and J. P. Hansen, *Physical Review E*, 2000, **61**, R1028–R1031.

17 S. Asakura and F. Oosawa, *The Journal of Chemical Physics*, 1954, **22**, 1255–1256.

18 A. Vrij, *Pure and Applied Chemistry*, 1976, **48**, 471–483.

19 B. Neu and H. J. Meiselman, *Biophysical Journal*, 2002, **83**, 2482–2490.

20 G. M. Artmann and S. Chien, *Bioengineering in cell and tissue research*, Springer Berlin Heidelberg, Berlin, Heidelberg, 2008, pp. 1–693.

21 D. A. Fedosov, W. Pan, B. Caswell, G. Gompper and G. E. Karniadakis, *Proceedings of the National Academy of Sciences*, 2011, **108**, 11772–11777.

22 Z. Varga and J. W. Swan, *Journal of Rheology*, 2015, **59**, 1271–1298.

23 J. Bergenholtz, W. C. K. Poon and M. Fuchs, *Langmuir*, 2003, **19**, 4493–4503.

24 Z. Varga, V. Grenard, S. Pecorario, N. Taberlet, V. Dolique, S. Manneville, T. Divoux, G. H. McKinley and J. W. Swan, *Proceedings of the National Academy of Sciences*, 2019, **116**, 12193–12198.

25 D. E. Huang and R. N. Zia, *Journal of Colloid and Interface Science*, 2019, **554**, 580–591.

26 M. Laurati, G. Petekidis, N. Koumakis, F. Cardinaux, A. B. Schofield, J. M. Brader, M. Fuchs and S. U. Egelhaaf, *The Journal of Chemical Physics*, 2009, **130**, 134907.

27 A. Boromand, S. Jamali and J. M. Maia, *Soft Matter*, 2017, **13**, 458–473.

28 J. Dzubiella, H. Löwen and C. N. Likos, *Physical Review Letters*, 2003, **91**, 248301.

29 I. Sriram and E. M. Furst, *Soft Matter*, 2012, **8**, 3335.

30 Y. Xu, K. H. Choi, S. G. Nagella and S. C. Takatori, *Soft Matter*, 2023, **19**, 5692–5700.

31 A. S. Khair and J. F. Brady, *Proceedings of the Royal Society A: Mathematical, Physical and Engineering Sciences*, 2007, **463**, 223–240.

32 B. E. Dolata and R. N. Zia, *Journal of Fluid Mechanics*, 2018, **836**, 694–739.

33 A. R. Altenberger, M. Tirrell and J. S. Dahler, *The Journal of Chemical Physics*, 1986, **84**, 5122–5130.

34 R. I. Cukier, *Macromolecules*, 1984, **17**, 252–255.

35 R. J. Phillips, W. M. Deen and J. F. Brady, *AIChE Journal*, 1989, **35**, 1761–1769.

36 B. Amsden, *Macromolecules*, 1998, **31**, 8382–8395.

37 J. F. Brady, *The Journal of Chemical Physics*, 1993, **99**, 567–581.

38 J. F. Brady and M. Vicic, *Journal of Rheology*, 1995, **39**, 545–566.

39 T. M. Squires and J. F. Brady, *Physics of Fluids*, 2005, **17**, 1–21.

40 J. P. Hansen and I. R. McDonald, *Theory of Simple Liquids: With Applications to Soft Matter: Fourth Edition*, Elsevier, 2013, pp. 1–619.

41 R. Castañeda-Priego, A. Rodríguez-López and J. M. Méndez-Alcaraz, *Journal of Physics: Condensed Matter*, 2003, **15**, S3393–S3409.

42 J. Piasecki, L. Bocquet and J. P. Hansen, *Physica A: Statistical Mechanics and its Applications*, 1995, **218**, 125–144.

43 L. Bocquet, *American Journal of Physics*, 1997, **65**, 140.

44 L. Bocquet, *Acta Physica Polonica B*, 1998, **29**, 1551–1564.

45 F. Hecht and F. Hecht, *Journal of Numerical Mathematics*, 2012, **20**, 1–14.

46 J. D. Weeks, D. Chandler and H. C. Andersen, *The Journal of Chemical Physics*, 2003, **54**, 5237.

47 J. A. Anderson, J. Glaser and S. C. Glotzer, *Computational Materials Science*, 2020, **173**, 109343.

48 R. Wulfert, U. Seifert and T. Speck, *Soft Matter*, 2017, **13**, 9093.

49 E. Balkovsky, A. Fouxon and V. Lebedev, *Physical Review Letters*, 2000, **84**, 4765–4768.

50 D. L. Koch and G. Subramanian, *Journal of Non-Newtonian Fluid Mechanics*, 2006, **138**, 87–97.

51 O. G. Harlen and D. L. Koch, *Journal of Fluid Mechanics*, 1993, **252**, 187–207.

52 M. Yang, S. Krishnan and E. S. Shaqfeh, *Journal of Non-Newtonian Fluid Mechanics*, 2016, **233**, 181–197.

53 K. Kremer and G. S. Grest, *The Journal of Chemical Physics*, 1990, **92**, 5057–5086.

54 J. C. Crocker, M. T. Valentine, E. R. Weeks, T. Gisler, P. D. Kaplan, A. G. Yodh and D. A. Weitz, *Physical Review Letters*,

2000, **85**, 888–891.

55 T. M. Squires and T. G. Mason, *Annual Review of Fluid Mechanics*, 2010, **42**, 413–438.

56 A. P. Alivisatos, K. P. Johnsson, X. Peng, T. E. Wilson, C. J. Loweth, M. P. Bruchez and P. G. Schultz, *Nature 1996 382:6592*, 1996, **382**, 609–611.

57 P. J. Santos, T. C. Cheung and R. J. Macfarlane, *Nano Lett.*, 2019, **19**, 5774–5780.

58 C. A. Mirkin, R. L. Letsinger, R. C. Mucic and J. J. Storhoff, *Nature 1996 382:6592*, 1996, **382**, 607–609.

59 A. Coniglio, L. D. Arcangelis, E. D. Gado, A. Fierro and N. Sator, *Journal of Physics: Condensed Matter*, 2004, **16**, S4831–S4839.

60 M. Bantawa, W. A. Fontaine-Seiler, P. D. Olmsted and E. Del Gado, *Journal of Physics: Condensed Matter*, 2021, **33**, 414001.

61 Y. Jiang and R. Seto, *Nature Communications*, 2023, **14**, 2773.

62 R. N. Zia, B. J. Landrum and W. B. Russel, *Citation: Journal of Rheology*, 2014, **58**, 1121.

63 J. W. Swan, R. N. Zia and J. F. Brady, *Journal of Rheology*, 2014, **58**, 1–41.

64 J. W. Swan, *J. Rheo.*, 2014, **58**, 307–337.

65 I. M. De Schepper, H. E. Smorenburg and E. G. Cohen, *Physical Review Letters*, 1993, **70**, 2178–2181.

66 M. Foglino, A. N. Morozov, O. Henrich and D. Marenduzzo, *Physical Review Letters*, 2017, **119**, 208002.

67 A. E. Nel, L. Mädler, D. Velegol, T. Xia, E. M. V. Hoek, P. Somasundaran, F. Klaessig, V. Castranova and M. Thompson, *Nat. Mater.*, 2009, **8**, 542–557.